Robustness study of bandpass NGD behavior of ring-stub microstrip circuit under temperature variation

Hongyu Du, Fayu Wan, Sébastien Lalléchère, Wenceslas Rahajandraibe, Blaise Ravelo

Robustness Study of Bandpass NGD Behavior of Ring-Stub Microstrip Circuit Under Temperature Variation

Hongyu Du, Fayu Wan, *Member*, *IEEE*, Sébastien Lalléchère, *Member*, *IEEE*, Wenceslas Rahajandraibe, *Member*, and Blaise Ravelo, *Member*, *IEEE*

***Abstract*—This paper explores an original study of bandpass (BP) negative group delay (NGD) robustness applied to ring-stub passive circuit. The proof of concept (PoC) circuit is constituted by a ring associated to open-end stub implemented in microstrip technology. An innovative experimental setup of temperature room containing the NGD PoC connected to a vector network analyzer is described. Then, the electrothermal data of S-parameters are measured by varying the ambient or room temperature range from 20°C to 60°C, i.e., 40°C maximal variation. The empirical results of the group delay (GD), transmission and reflection coefficient mappings versus the couple (temperature, frequency) highlights how the temperature affects the BP NGD responses. An innovative electrothermal calibration technique by taking into account the interconnection cable influence is developed. The electrothermal robustness analysis is carried out by variations of the NGD center frequency, cut-off frequencies and value in function of the temperature.**

Index Terms*— *Bandpass NGD, microstrip circuit, temperature effect characterization, S-parameters analysis, robustness study, experimentation, electrothermal analysis.

I. Introduction

THE PRACTICAL EXISTENCE of the intriguing negative group delay (NGD) effect was initially experimented by physicists with optical system [1-4]. At the beginning, the observation of the NGD effect was made by using negative group velocity (NGV) dispersive media [1-2]. The analytical study of the NGD effect is necessary for the basic physical interpretation. Then, the NGD function existence at the microwave wavelength becomes an attractive topic for electronic design and research engineers [5-12].

The remarkable period of the NGD function development in the microwave area has been found during the design of metamaterial artificial transmission line (TL) exhibiting negative refractive index effect [5-8]. The metamaterial based NGD circuits were designed with periodical structures [6, 8]. Diverse microwave NGD devices operating as quad-band circuits [7], reconfigurable circuits with tunable metamaterial resonators [11], and resistive lossy left-handed TLs [12] were proposed. It was emphasized that some NGD circuits are susceptible to propagate pulse signals with superluminal effect [13-16]. Moreover, the superluminal effect was experimented with different systems with optimal behavior [14], two interference pulses [15], and active circuit approach [16]. Nevertheless, the existence of the NGD function and superluminal effect is not in contradiction with the causality [17-18]. Such counterintuitive and extraordinary effect observation raises curious questions on the meaning and interpretation of the NGD function in the electronic and microwave engineering. Therefore, a simple theorization of NGD function based on the analogy with the filter function was initiated [19].

Innovative NGD circuits operating with low-pass and bandpass behaviors were designed. Thanks to the ambitious research work made by some research group around the world, various topologies of typical bandpass NGD circuits were investigated [20-29]. The main challenges on the NGD microwave circuit of the last two decades were on the loss compensation [20-21], circuit operation understanding [22-23], the size reduction [24-27], and the implementation of low-attenuation passive circuits [28-29] susceptible to operate in the gigahertz frequency range. An active NGD circuit designed with microwave transversal filter approach was proposed [20]. To highlight the NGD design feasibility of some microstrip

Manuscript received xxx xx, 2021; revised xxx xx, 2021; accepted xxx xx, 2021. Date of publication xxx xx, 2021. (Corresponding author: Dr. Yang Liu)

This research work was supported in part by NSFC under Grant 61971230, and in part by Jiangsu Specially Appointed Professor program and Six Major Talents Summit of Jiangsu Province (2019-DZXX-022) and in part by the Startup Foundation for Introducing Talent of NUIST.

Fayu Wan, Hongyu Du and Blaise Ravelo are with the Nanjing University of Information Science & Technology (NUIST), Nanjing 210044, Jiangsu, China (E-mail: {fayu.wan, blaise.ravelo}@nuist.edu.cn, 614920361 @qq.com).

Yang Liu is with Altran, 78140 Vélizy-Villacoublay, France. (E-mail: liuyang2101@gmail.com).

Lala Rajaoarisoa is with IMT Lille Douai, Univ. Lille, Unité de Recherche en Informatique et Automatique, F-59000 Lille, France. (E-mail: lala.rajaoarisoa@imt-lille-douai.fr).

Sébastien Lalléchère is with Université Clermont Auvergne, Institut Pascal, SIGMA Clermont, France. (E-mail: sebastien.lallechere@uca.fr).

Wenceslas Rahajandraibe is with the Aix-Marseille University, CNRS, University of Toulon, IM2NP UMR7334, Marseille, France (E-mail: wenceslas.rahajandraibe@im2np.fr).

Preeti Thakur, and Atul Thakur are with the Amity University Haryana, Gurgaon, 122413 India (E-mail: pthakur@ggn.amity.edu, athakur1@ggn.amity.edu).

Glauco Fontgalland is with Federal University of Campina Grande, Applied Electromagnetic and Microwave Lab., Campina Grande/PB, 58429, Brazil. (E-mail: fontgalland@dee.ufcg.edu.br).

topologies, an absorptive bandstop filter based [21] and signal interference [22] based NGD circuit were introduced. Furthermore, different NGD compact circuits based on microstrip TLs were investigated [24-27]. Then, innovative geometrical shape topologies of low loss NGD passive microstrip circuits were proposed [28-29]. Some tentative applications of NGD function targeted for the GD equalization were initiated [30-31].

Behind the progress of the microwave circuit design, further curious questions remain to be answered. For example, we would like to study the temperature effect on the NGD microstrip circuit as investigated in [32-34]. The paper is organized in four main sections as follows:

- Section II introduces the design of the proof of concept (PoC) of the BP NGD circuit constituted by the combined ring and stub microstrip structure.
- Section III investigates the experimental setup on the BP NGD circuit under test (CUT) of the empirical robustness study. The guideline of the innovative electrothermal test operation process with the calibration technique of the temperature room will be explained.
- Section IV discusses on the observable results of the robustness study. The electrothermal empirical results illustrating the NGD performances versus the ambient temperature will be examined which show the variation of the BP NGD responses.
- Then, Section V is the final conclusion.

II. Design Description of the Ring-Stub BP NGD Circuit

This section describes the design and implementation of the PoC prototype. The BP NGD circuit is designed by modification of parallel line topology [28]. Then, the performance was optimized in function of the positioning and the physical length of an open-ended stub.

A. PoC of Microstrip Circuit Design

The considered PoC is a two-port distributed passive circuit. As illustrated by the 2-D design shown by Fig. 1(a), the circuit is constituted by two microstrip circular lines presenting physical inner radius, R_1, outer radius, R_2 and width, w. The two circular lines are connected in parallel. The access lines have physical length, l_{port} and width, w_{port}.

The top circular line is connected to open ended straight stub having physical length, l_1, and width, w_1, at its mid-point. The physical parameters of this PoC prototype are indicated in Table I. The fabricated circuit prototype photographed in Fig. 1(b) is implemented on Cu-metalized FR4 dielectric substrate in microstrip technology. The substrate physical characteristics are addressed by Table II.

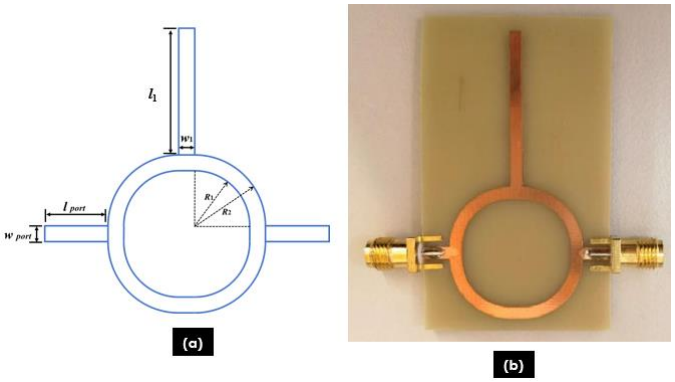

Fig. 1. (a) 2-D design and (b) photo of the ring-stub circuit under study.

TABLE I
GEOMETRICAL PARAMETERS OF THE CIRCUIT POC

Circuit	Description	Parameter	Value
Whole circuit	Total length	L	58.2 mm
	Total width	w	35 mm
Access line	Length	l_{port}	5 mm
	Width	w_{port}	2.8 mm
Stub	Length	w_1	2.2 mm
	Width	l_1	28 mm
Ring	Inner radius	R_1	9.5 mm
	Outer radius	R_2	11.5 mm

TABLE II
PHYSICAL PARAMETERS OF THE POC CIRCUIT SUBSTRATE

Structure	Description	Parameters	Values
Substrate	Relative permittivity	ε_r	4.5
	Loss tangent	$\tan(\delta)$	0.02
	Thickness	h	1.6 mm
Metallization conductor	Copper conductivity	σ	58 MS/m
	Thickness	t	35 µm

B. BP NGD Function Specifications

The analysis of the ring-stub passive symmetric circuit is based on the 2-D frequency-dependent S-matrix:

$$[S(j\omega)] = \begin{bmatrix} S_{11}(j\omega) & S_{21}(j\omega) \\ S_{21}(j\omega) & S_{11}(j\omega) \end{bmatrix} \quad (1)$$

with the angular frequency, ω. The main parameters are basically the transmission coefficient magnitude, and the reflection coefficient, respectively:

$$S_{21}(\omega) = |S_{21}(j\omega)| \quad (2)$$

$$S_{11}(\omega) = |S_{11}(j\omega)| . \quad (3)$$

Then, the essential parameter is the GD defined by:

$$GD(\omega) = -\partial \arg[S_{21}(j\omega)] / \partial\omega . \quad (4)$$

Fig. 2(a) represents the GD response of BP NGD ideal circuit. This BP NGD function is characterized by the cut-off angular frequencies, $\omega_1<\omega_2$, with:

$$GD(\omega_1 < \omega < \omega_2) < 0 . \quad (5)$$

The associated NGD bandwidth (BW) is given by:

$$\Delta\omega = \omega_2 - \omega_1 . \quad (6)$$

The response is also characterized by a center angular frequency $\omega_1 < \omega_0 < \omega_2$ which can be defined by:

$$GD(\omega_0) = GD_0 < 0 . \quad (7)$$

The behavior of the transmission coefficient characterized by attenuation limit:

$$S_{21}(\omega_0) = A \quad (8)$$

is presented by Fig. 2(b). Then, the access matching can be limited with respect to the diagram of Fig. 2(c) by:

$$S_{11}(\omega_0) = B . \quad (9)$$

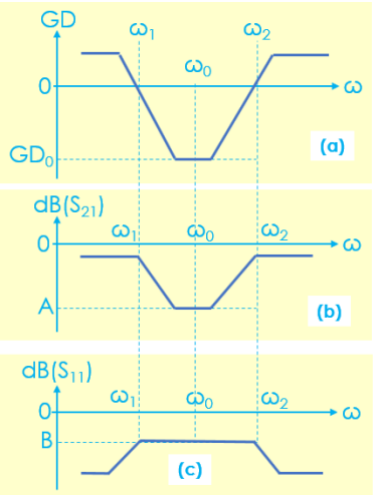

Fig. 2. BP NGD circuit ideal responses: (a) *GD*, (b) S_{21} and (c) S_{11}.

These specifications will serve to the BP NGD electrothermal characterization in the rest of the paper.

To investigate the electrothermal NGD behavior of the circuit, an innovative experimental setup described in the following section was considered.

III. Experimental Setup of the Robustness Study Applied to the Ring-Stub Circuit

The present section describes the robustness study empirical principle. The PoC of the robustness is based on the electrothermal analysis of the ring-stub NGD circuit. The experimental setup will be introduced in the following subsection.

A. Principle of the Experimental Setup for the NGD Electrothermal Analysis

The electrothermal empirical study principle of microwave circuit is fundamentally aimed to determine the transmission and reflection coefficients of S-matrix proposed in equation (1) with the evolution of ambient temperature, *T*:

$$[S(jf,T)] = \begin{bmatrix} S_{11}(jf,T) & S_{21}(jf,T) \\ S_{21}(jf,T) & S_{11}(jf,T) \end{bmatrix} . \quad (10)$$

It means that the empirical S-parameter data should be expressed in function of couple $(j\omega = j2\pi f, T)$. To measure the S-parameters, we proposed the innovative experimental setup highlighted by illustrative diagram in Fig. 3. The vector network analyzer (VNA) is facing the side of the test box. After calibration, two ports are respectively connected with a 1m-long cable. The cable enters the test box through the hole on the side of the test box. At the same time, the two cables are relatively parallel and do not cross for a certain distance to avoid mutual interference. After putting it into the test chamber, fix both ends of the cable on the iron frame inside the test chamber with adhesive tape, and fix the thermometer. After placing, close the door of the test chamber to start the test. Of course, the VNA apparatus is needed to record the S-parameters. The thermal room specifications will be described in the following subsection.

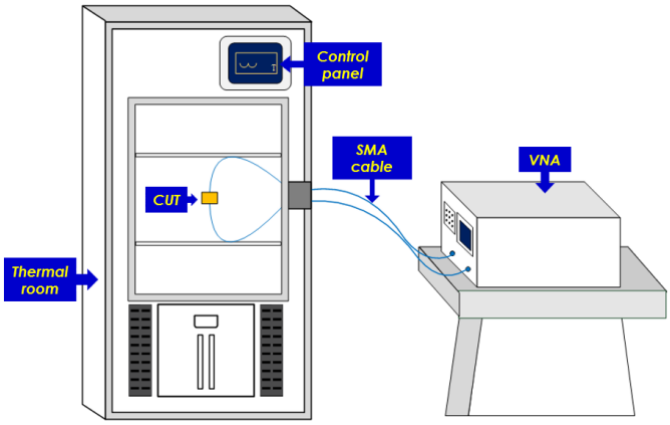

Fig. 3. Illustrative diagram of NGD electrothermal test.

B. Electrothermal Test and the Thermal Room Specification

Fig. 4 shows the photograph of the electrothermal test setup. The employed VNA is referenced Agilent® AV3672B-S, which operates from 10 MHz to 26.5 GHz. We use two identical SMA cables 1meter-length. Then, the main innovative part of this research work is the consideration of the thermal room with volume 1 m × 1 m × 1 m. This later one is referenced ESPEC® [35]. During the experimentation, the circuit under test (CUT) is placed in the room as indicated in Fig. 4. Then, it is connected to the VNA as previously depicted in Fig. 3. Prior to running the test, the VNA was calibrated in SOLT configuration at the ambient temperature, T_a=20°C. We underline that the present study is limited to the case of temperature, *T*, higher than T_a.

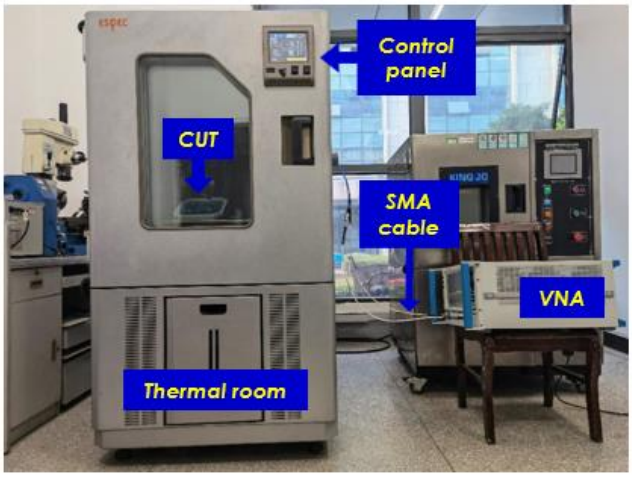

Fig. 4. Photo of the considered electrothermal experimental setup.

Then, we realize that such a calibration remains valid to measure the circuit with the variation of the room temperature, $\Delta T=T-T_a<100°C$. Moreover, the influence of the room temperature on the interconnection cables and CUT connectors is negligible.

C. Guideline of the Thermal Room Test Operation

The thermal room test operation can be summarized by the following steps:

- **Step A**: Installation with respect to the diagram shown by Fig. 3. This step requires the familiarization to the use of VNA and the control of the temperature (alternating humidity and heat) with the thermal test chamber.
- **Step B:** Connect the extension cable and put it into the high and low temperature (alternating humidity and heat) test chamber without test circuit to ensure that the two cables entering the temperature chamber are equal length and parallel. Close the thermal room and connect the NGD circuit to be tested on the no-load cable.
- **Step C**: VNA calibration with respect to the range of the frequency of the CUT.
- **Step D**: Measure the S-parameters of the cable with the temperature change when no load.
- **Step E**: Adjust the room temperature and wait for the temperature stabilization.
- **Step F**: Adjust the temperature box, the range of each rise is 4°C within the time of 5 minutes. After reaching a rise, keep the temperature stable during 1 minute. Then, derive the S-parameter data from the VNA.
- **Step G**: The previous step must be repeated until the temperature variation reaches 40°C. For the present case of study, the users must save 11 groups of ring-stub circuit S-parameter data family.

To verify the feasibility of the robustness analysis of the NGD circuit under ambient temperature stress, practical investigation will be presented in the next section.

IV. Investigation on the Results of the BP NGD Electrothermal Experimentation

The present section deals with the examination of the ring-stub circuit electrothermal test results. The BP NGD validation based on the comparison between simulation and measurement is presented. Then, the BP NGD responses will be discussed in function of the ambient temperature variation.

A. Preliminary Validation of the BP NGD Behavior of the Ring-Stub Circuit

To validate the BP NGD behavior of the CUT, comparisons between the simulated ("Sim.") and measured ("Meas.") results were carried out in the frequency band from 2.35 GHz to 2.5 GHz. The simulated results were obtained from the commercial tool of electronic and RF/microwave circuit simulator ADS® from Keysight Technologies®. The ring-stub circuit operates as dual-band NGD function. The simulated, and measured GDs and magnitudes of the reflection and transmission coefficients are plotted in Fig. 5(a) and in Fig. 5(b), respectively. It can be pointed out that these comparative results present a very good agreement. In addition, the simulated and measured GD responses are plotted in Fig. 5(c). These results confirm that the ring stub CUT behaves as a BP NGD function. Table III presents the comparison between the simulated and experimented results of BP NGD specifications. As expected, the CUT exhibits NGD center frequency of approximately f_0=2.42 GHz and NGD value, $GD(f_o)$, of -1.9 ns. It can be seen from Fig. 5(b) that in the test frequency band, the attenuation remains better than –4 dB and the reflection coefficient is better than -11 dB. The slight frequency shifts of NGD center frequency are mainly due to the fabrication inaccuracies, substrate effective permittivity tolerance, and losses versus the numerical computation accuracy.

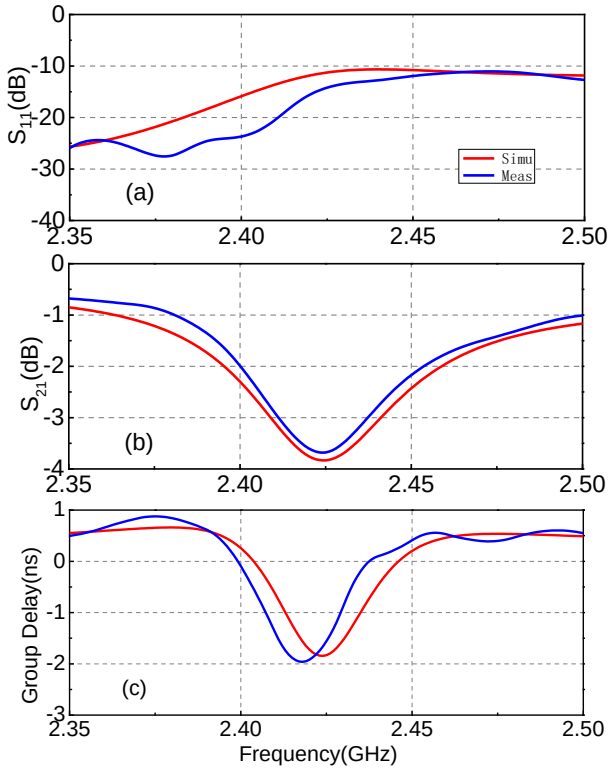

Fig. 5. (a) Reflection and (b) transmission coefficients and (c) GD responses of the ring-stub CUT prototype shown by Figs. 1 in the second bandwidth at ΔT=0.

TABLE III
COMPARISON OF BP NGD SPECIFICATIONS FROM THE RING-STUB CUT

Approach	f_0 (GHz)	$GD(f_0)$ (GHz)	BW (MHz)	$S_{21}(f_0)$ (dB)	$S_{11}(f_0)$ (dB)
Simu.	2.424	-1.85	42.7	-3.83	-11.2
Meas.	2.418	-1.97	38.5	-3.68	-15.9

The electrothermal test results of the ring-stub circuit were generated with respect to the guideline indicated in Subsection III-C. The experimented data results obtained after the post-processing will be analyzed in the two following subsections.

B. Interconnection Cable Calibration Including the Temperature Stress Effect

Before the NGD characterization of the ring-stub circuit, the interconnection cable was separately calibrated at each sample of the room temperature variation, ΔT, was progressively increased from 0°C to 40°C step 1°C. During the test, the VNA was calibrated from 2.3 GHz and 2.6 GHz to generate the

thermal and frequency dependent S-parameters of the employed interconnection cable which can be denoted:

$$[S_{cable}(jf,T)] = \begin{bmatrix} S_{11cable}(jf,T) & S_{21cable}(jf,T) \\ S_{21cable}(jf,T) & S_{11cable}(jf,T) \end{bmatrix}. \quad (11)$$

The associated GD determined from the transmission coefficient is given by:

$$GD_{cable}(f,T) = \frac{-\partial \arg[S_{21cable}(jf,T)]}{2\pi\,\partial f}. \quad (12)$$

Consequently, the obtained electrothermal mappings of the employed interconnection cable GD, transmission and reflection coefficients are displayed in Fig. 6(a), Fig. 6(b) and, Fig. 6(c), respectively. Significant variations of the interconnection cable S-parameter magnitudes can be observed. The NGD center frequency, f_0, of the ring-stub circuit under temperature stress is considered to carry out the calibration. Accordingly, we consider the $GD(f_0)$, $S_{21}(f_0)$, and $S_{11}(f_0)$ empirical data of the tested cable summarized in Table IV. The influence of the interconnection cable can be quantified from this table. It can be emphasized from this empirical result that the cable response presents the variations of:

- Interconnect cable GD presenting medium value of about mean($GD_{cable}(f_o)$)≈9.1 ns and variation max($GD_{cable}(f_o)$)-min($GD_{cable}(f_o)$)<0.1 ns,
- Transmission coefficient having absolute variations of about max($S_{21cable}(f_o)$)-min($S_{21cable}(f_o)$)<0.2 dB,
- And reflection coefficient with maximal value max($S_{11cable}(f_o)$) lower than -23 dB.

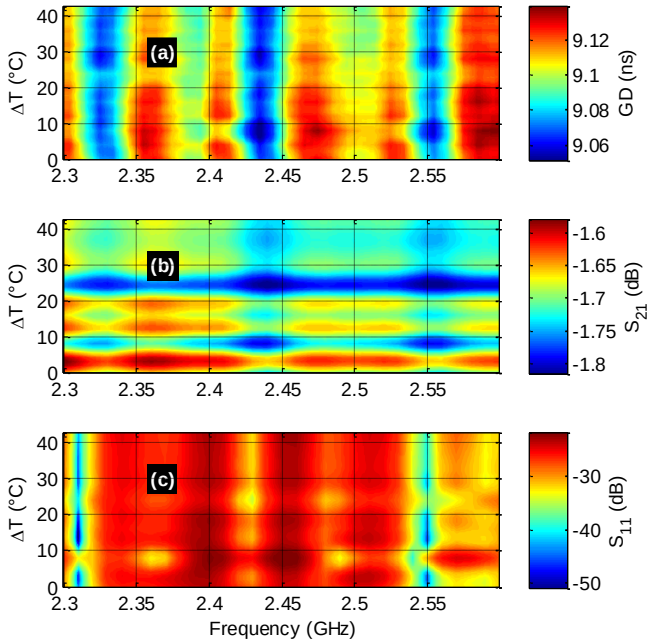

Fig. 6. Mappings of (a) *GD*, (b) S_{21} and (c) S_{11} for the interconnection cable versus frequency and temperature effect.

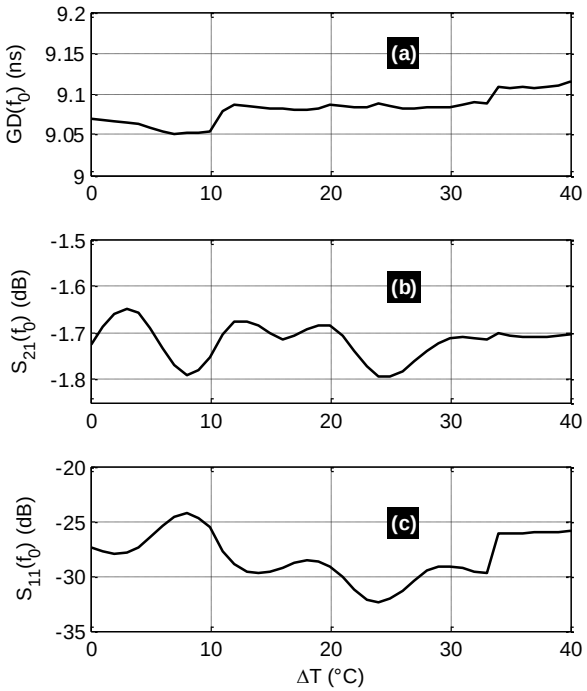

Fig. 7. (a) *GD*, (b) S_{21} and (c) S_{11} of the interconnection cable at NGD center frequencies versus temperature effect.

TABLE IV
GD, TRANSMISSION AND REFLECTION COEFFICIENTS AT THE NGD CENTRE FREQUENCY OF THE INTERCONNECTED CABLE

ΔT (°C)	f_0 (GHz)	$GD(f_0)$ (ns)	$S_{21}(f_0)$ (dB)	$S_{11}(f_0)$ (dB)
0	2.434	9.070	-1.725	-27.329
4	2.434	9.064	-1.658	-27.360
8	2.432	9.052	-1.792	-24.292
12	2.429	9.086	-1.676	-28.924
16	2.427	9.082	-1.715	-29.243
20	2.426	9.086	-1.684	-29.135
24	2.425	9.088	-1.794	-32.331
28	2.423	9.084	-1.738	-29.512
32	2.421	9.090	-1.711	-29.587
36	2.418	9.109	-1.709	-26.062
40	2.416	9.115	-1.704	-25.918

By taking into account the results of the cable calibration, the BP NGD characterization of the ring-stub circuit including the electrothermal robustness analysis will be discussed in the following paragraph.

C. BP NGD Characterization After Processing at Ambient Temperature on the Ring-Stub Circuit

The heart of the thermal stress robustness investigation is explored in the present subsection. The robustness study of the BP NGD CUT is focused around the NGD frequency band. We choose the operation frequency band between 2.35 GHz and 2.5 GHz. The following paragraph explains the calibration approach by considering the cable electrothermal effect.

1) NGD Circuit Calibration Approach by Taking Into Account the Cable Electrothermal Effect Response

The electrothermal observable data processing is elaborated from the measurement of the total circuit composed of the interconnection cable characterized in the previous subsection connected to the CUT. Accordingly, the total circuit S-parameters can be denoted by:

$$\left[S_{total}(jf,T)\right]=\begin{bmatrix} S_{11total}(jf,T) & S_{21total}(jf,T) \\ S_{21total}(jf,T) & S_{11total}(jf,T) \end{bmatrix}. \quad (13)$$

As the interconnection cable with S-parameters given by equation (11) and the tested circuit with S-parameters given by equation (10) are very well matched in the NGD frequency band, we can deduce the CUT transmission coefficient from the following relation:

$$S_{11}(jf,T)\approx S_{11total}(jf,T) \quad (14)$$

$$S_{21}(jf,T)\approx \frac{S_{21total}(jf,T)}{S_{21cable}(jf,T)}. \quad (15)$$

It can be derived from equation (14) that the ring-stub CUT measured GD and transmission coefficient magnitude in decibel are respectively expressed by:

$$GD(f,T)\approx GD_{total}(f,T)-GD_{cable}(f,T) \quad (16)$$

$$S_{21_{dB}}(f,T)\approx S_{21total_{dB}}(f,T)-S_{21cable_{dB}}(f,T). \quad (17)$$

Based on the proposed approach, the empirical results are examined in the following paragraph.

2) Electrothermal Data Mapping Processing of the Ring-Stub CUT

The thermal stress measurement of the ring-stub circuit was carried out by including the interconnect cable. The experimented data represented by S-parameter equation (10) were recorded after 11 minutes of the temperature change. After the thermal stress, the BP NGD characterization of the ring NGD circuit is performed by using previously suggested equations (13), (15), and (16). Similar to the analysis of the previous subsection, the analyses were based on the mappings of the ring-stub CUT GD, transmission and reflection coefficients displayed by Fig. 8(a), Fig. 8(b), and Fig. 8(c), respectively. As expected, an interesting electrothermal effect is curiously observed. It can be seen in Fig. 8(a) that the ring-stub circuit conserve the BP NGD behavior despite the thermal stress. However, the NGD value and the NGD center frequency are decreasing inversely to the temperature variation. Moreover, it can be underlined from Fig. 8(a) that the NGD bandwidth is slightly increasing. Furthermore, in the NGD frequency range, despite the temperature stress, at the NGD center frequency, the attenuation depicted by Fig. 8(b) remains better than 3 dB and the ring-stub circuit access matching illustrated by Fig. 8(c) remains better than -11 dB.

In addition, similar to the normal operation of BP NGD circuits available in the literature, the transmission coefficient magnitude presents an electrothermal behavioral effect shown by Fig. 8(b) similar to the GD of Fig. 8(a). Based on the explored raw data, the robustness study related to the BP NGD specifications of the ring-stub NGD circuit will be examined in the following paragraph.

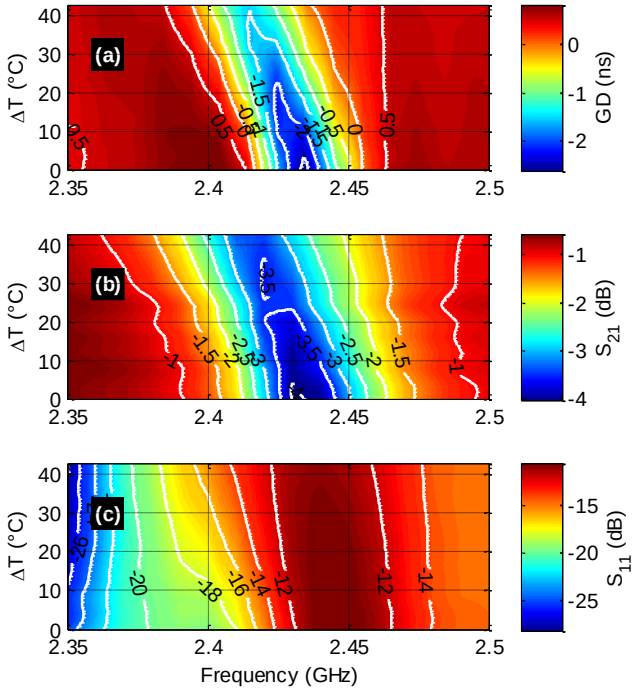

Fig. 8. Mappings of experimented (a) *GD*, (b) S_{21} and (c) S_{11} of ring-stub circuit versus (*f*,*T*).

3) Robustness related to the BP NGD specifications

In the area of electronic and microwave engineering, the robustness study must be referenced by observable data. For the present study, we are presenting a BP NGD behavior of a microstrip circuit against the thermal stress. For the best of the authors' knowledge, this is the first study of electrothermal BP characterization applied to microstrip circuit.

As aforementioned by Figs. 2, the BP NGD specifications are quantified by the NGD center frequency, NGD value, NGD bandwidth, attenuation and reflection coefficient of the CUT. Based on the data depicted in Figs. 8, we extracted the NGD center frequency, NGD value, and NGD bandwidth versus stress temperature which are plotted in Fig. 9(a), Fig. 9(b) and Fig. 9(c), respectively. Then, the variations of the transmission coefficient, reflection coefficient, and insertion loss flatness versus stress temperature are shown in Fig. 10(a), Fig. 10(b), and Fig. 10(c).

The overall BP NGD specifications are characterized by the NGD center frequency, f_0, BW, $\Delta f = f_2 - f_1$, value, $GD(f_0)$, attenuation, $S_{21_{dB}}(f_0)$, matching, $S_{21_{dB}}(f_0)$, and insertion loss flatness, $S_{21_{dB}}(f_1)-S_{21_{dB}}(f_0)$ and $S_{21_{dB}}(f_2)-S_{21_{dB}}(f_0)$. Table V recapitulates the quantified BP NGD characteristics of the ring-stub circuit under temperature variation from 0°C to 40°C with step of 4°C.

TABLE V
BP NGD SPECIFICATIONS OF THE RING-STUB CUT VERSUS TEMPERATURE

ΔT (°C)	f_0 (GHz)	Δf (MHz)	$GD(f_0)$ (ns)	$S_{21}(f_0)$ (dB)	$S_{11}(f_0)$ (dB)	$S_{21}(f_1)$-$S_{21}(f_0)$ (dB)	$S_{21}(f_2)$-$S_{21}(f_0)$ (dB)
0	2.434	39	-2.914	-4.176	-11.5	1.52	1.45
4	2.434	40	-2.746	-4.098	-11.34	1.46	1.46
8	2.432	40	-2.549	-3.798	-11.26	1.35	1.44
12	2.429	42	-2.472	-3.947	-12.71	1.26	1.21
16	2.427	43	-2.440	-3.805	-12.44	1.33	1.28
20	2.426	44	-2.327	-3.762	-12.23	1.37	1.26
24	2.425	43	-2.181	-3.599	-12.26	1.33	1.17
28	2.423	42	-2.003	-3.602	-12.12	1.19	1.11
32	2.421	43	-1.822	-3.577	-12	1.18	1.03
36	2.418	44	-1.749	-3.511	-13.25	1.11	0.92
40	2.416	44	-1.653	-3.438	-13.1	1.08	0.95

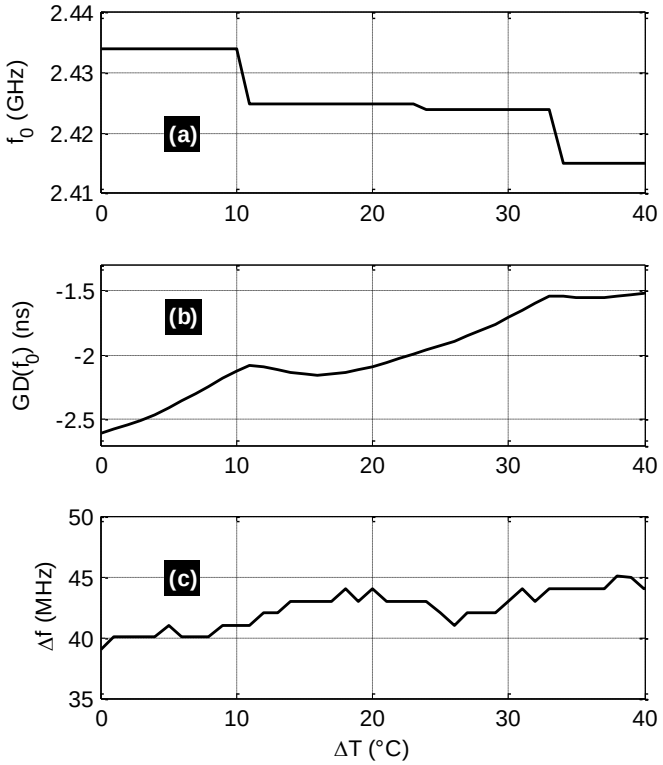

Fig. 9. Plots of NGD (a) center frequency, (b) value and (c) bandwidth versus temperature parameter after test processing of ring-stub circuit.

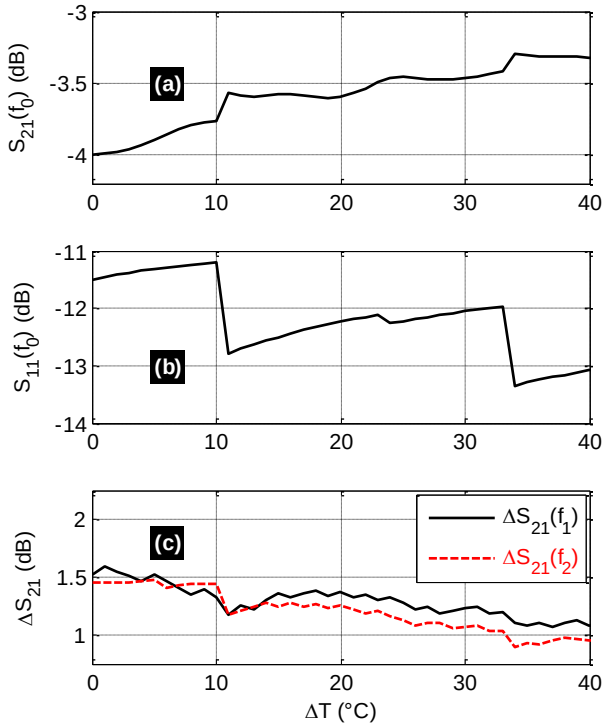

Fig. 10. (a) Transmission and (b) reflection coefficients at the NGD center frequency, and (c) attenuation flatness versus temperature of the ring-stub circuit after test processing value.

It is noteworthy from Table V that the attenuation and access matching are still better than 4 dB and 11 dB despite the stress. However, we can point out that:

- The NGD centre frequency presents a shift of about: $\max(f_0) - \min(f_0) = 18\ MHz$,
- And the GD maximal variation is of about: $\max[GD(f_0)] - \min[GD(f_0)] = 1.26\ ns$.

D. Discussion on the Application of BP NGD Robustness Study of the Ring-Stub CUT

These previous empirical results enable to qualify the BP NGD robustness of the ring-stub circuit. The main robustness risk related to such results should be specified in function of the electronic system applications. For example, for the case of IEEE 802.11a/b wireless transceiver system, the standard communication channel bandwidths are higher than 20 MHz. Therefore, we can expect that the NGD circuit robustness can

induce tolerable operation within the ambient temperature variation, ΔT, less than 40°C.

V. Conclusion

An original study of BP NGD microstrip circuit, never being achieved before, is investigated. The study is based on the test of ring-stub microstrip circuit. After the recall on the BP NGD specifications, the NGD design of the proof of concept is described. Then, the electrothermal test guideline is explained with the consideration of the experimental setup of the thermal room and the VNA calibration.

The robustness of the ring-stub circuit is validated by the empirical test under temperature fluctuation with maximal amplitude of about 40°C. The variation of the BP NGD characteristics as the NGD center frequency, NGD value, transmission and reflection coefficients in function of the temperature are discussed.

The proposed study is useful for the future application of the BP NGD circuit robustness and also reliability in the electronic system susceptible to operate in the wide range of ambient temperature variation.

References

[1] S. Chu and S. Wong, “Linear Pulse Propagation in an Absorbing Medium,” Phys. Rev. Lett., Vol. 48, 1982, pp. 738-741.

[2] B. Ségard and B. Macke, “Observation of Negative Velocity Pulse Propagation,” Phys. Lett. A, Vol. 109, pp. 213-216, 1985.

[3] B. Macke and B. Ségard, “Propagation of light-pulses at a negative group-velocity,” Eur. Phys. J. D, vol. 23, pp. 125-141, 2003.

[4] J. N. Munday and W. M. Robertson, “Observation of Negative Group Delays within a Coaxial Photonic Crystal Using an Impulse Response Method,” Optics Communications, Vol. 273, No. 1, 2007, pp. 32-36.

[5] G. V. Eleftheriades, O. Siddiqui, and A. K. Iyer, “Transmission Line for Negative Refractive Index Media and Associated Implementations without Excess Resonators,” IEEE Microw. Wireless Compon. Lett., Vol. 13, No. 2, pp. 51-53, Feb. 2003.

[6] O. F. Siddiqui, M. Mojahedi and G. V. Eleftheriades, “Periodically Loaded Transmission Line With Effective Negative Refractive Index and Negative Group Velocity,” IEEE Trans. Antennas Propagat., Vol. 51, No. 10, Oct. 2003, pp. 2619-2625.

[7] O. F. Siddiqui, S. J. Erickson, G. V. Eleftheriades, and M. Mojahedi, “Time-Domain Measurement of Negative-Index Transmission-Line Metamaterials,” IEEE Trans. Microw. Theory Techn., Vol. 52, No. 5, pp. 1449-1453, May 2004.

[8] T. Kokkinos, C. D. Sarris and G. V. Eleftheriades, "Periodic finite-difference time-domain analysis of loaded transmission-line negative-refractive-index metamaterials," in IEEE Transactions on Microwave Theory and Techniques, vol. 53, no. 4, pp. 1488-1495, Apr. 2005.

[9] L. Markley and G. V. Eleftheriades, “Quad-Band Negative-Refractive-Index Transmission-Line Unit Cell with Reduced Group Delay,” Electronics Letters, Vol. 46, No. 17, Aug. 2010, pp. 1206-1208.

[10] G. Monti and L. Tarricone, “Negative Group Velocity in a Split Ring Resonator-Coupled Microstrip Line,” Progress In Electromagnetics Research, Vol. 94, pp. 33-47, 2009.

[11] T. Nesimoglu and C. Sabah, “A Tunable Metamaterial Resonator Using Varactor Diodes to Facilitate the Design of Reconfigurable Microwave Circuits,” IEEE Trans. CAS II: Express Briefs, Vol. 63, No. 1, Jan. 2016, pp. 89-93.

[12] J. J. Barroso, J. E. B. Oliveira, O. L. Coutinho and U. C. Hasar, “Negative group velocity in resistive lossy left-handed transmission lines,” IET Microwaves, Antennas & Propagation, Vol. 10, No. 7, May 2016, pp. 808-815.

[13] H. Cao, A. Dogariu, and L. J. Wang, "Negative group delay and pulse compression in superluminal pulse propagation," IEEE J. Sel. Top. Quantum Electron., Vol. 9, No. 1, 52-58, 2003.

[14] B. Macke, B. Ségard, and F. Wielonsky, “Optimal superluminal systems,” Phys. Rev. E 72, 035601(R) (2005).

[15] B. Ségard and B. Macke, “Two-pulse interference and superluminality,” Optics Communications 281 (2008), pp. 12–17.

[16] M. Kitano, T. Nakanishi, and K. Sugiyama, “Negative group delay and superluminal propagation: An electronic circuit approach,” IEEE J. Selected Topics in Quantum Electronics, vol. 9, no. 1, pp. 43-51, Jan.-Feb. 2003.

[17] M. W. Mitchell, and R. Y. Chiao, “Negative group delay and "fronts" in a causal system: An experiment with very low frequency bandpass amplifiers,” Phys. Lett. A, vol. 230, no. 3-4, pp. 133-138, June 1997.

[18] M. W. Mitchell and R.Y. Chiao, “Causality and Negative Group-delays in a Simple Bandpass Amplifier,” Am. J. Phys., vol. 66, 1998, pp. 14-19.

[19] B. Ravelo, “Similitude between the NGD function and filter gain behaviours,” International Journal of Circuit Theory and Applications (Int. J. Circ. Theor. Appl.), Vol. 42, No. 10, Oct. 2014, pp. 1016–1032.

[20] C.-T.-M. Wu and T. Itoh, “Maximally flat negative group-delay circuit: A microwave transversal filter approach,” IEEE Trans. Microw. Theory Techn., vol. 62, no. 6, pp. 1330-1342, Jun. 2014.

[21] T. Zhang, R. Xu and C. M. Wu, “Unconditionally Stable Non-Foster Element Using Active Transversal-Filter-Based Negative Group Delay Circuit,” IEEE Microw. Wireless Compon. Lett., vol. 27, no. 10, pp. 921-923, Oct. 2017.

[22] L.-F. Qiu, L.-S. Wu, W.-Y. Yin, and J.-F. Mao, “Absorptive bandstop filter with prescribed negative group delay and bandwidth,” IEEE Microw. Wireless Compon. Lett., vol. 27, no. 7, pp. 639-641, Jul. 2017.

[23] Z. Wang, Y. Cao, T. Shao, S. Fang and Y. Liu, “A Negative Group Delay Microwave Circuit Based on Signal Interference Techniques,” IEEE Microw. Wireless Compon. Lett., vol. 28, no. 4, pp. 290-292, Apr. 2018.

[24] G. Liu and J. Xu, “Compact transmission-type negative group delay circuit with low attenuation,” Electron. Lett., vol. 53, no. 7, pp. 476-478, Mar. 2017.

[25] T. Shao, Z. Wang, S. Fang, H. Liu, and S. Fu, “A compact transmission line self-matched negative group delay microwave circuit,” IEEE Access, vol. 5, no. 1, pp. 22836-22843, Oct. 2017.

[26] G. Chaudhary, Y. Jeong and J. Lim, “Miniaturized dual-band negative group delay circuit using dual-plane defected structures,” IEEE Microwave Wireless Compon. Lett., vol. 21, no.1, pp.19-21, Jan. 2011.

[27] T. Shao, S. Fang, Z. Wang and H. Liu, “A Compact Dual-Band Negative Group Delay Microwave Circuit,” Radio Engineering, vol. 27, no. 4, pp. 1070-1076, Dec. 2018.

[28] F. Wan, N. Li and B. Ravelo, “O=O Shape Low-Loss Negative Group Delay Microstrip Circuit,” IEEE Transactions on Circuits and Systems II: Express Briefs, Vol. 67, No. 10, Oct. 2020, pp. 1795-1799.

[29] X. Zhou, T. Gu, L. Wu, F. Wan, B. Li, N. M. Murad, S. Lalléchère, and B. Ravelo, “S-Matrix and Bandpass Negative Group Delay Innovative Theory of Ti-Geometrical Shape Microstrip Structure,” IEEE Access, Vol. 8, No. 1, 2020, pp. 160363-160373.

[30] K.-P. Ahn, R. Ishikawa and K. Honjo, “Group Delay Equalized UWB InGaP/GaAs HBT MMIC Amplifier using Negative Group Delay Circuits,” IEEE Trans. Microw. Theory Techn., vol. 57, no. 9, Sept. 2009, pp. 2139- 2147.

[31] T. Shao, Z. Wang, S. Fang, H. Liu and Z. Chen, “A Full-Passband Linear-Phase Band-Pass Filter Equalized with Negative Group Delay Circuits,” IEEE Access, vol. 8, Feb. 2020, pp. 43336-43343.

[32] B. Ravelo, A. Thakur, A. Saini and P. Thakur, “Microstrip dielectric substrate material characterization with temperature effect”, ACES Journal, Vol. 30, No. 12, Dec. 2015, pp. 1322-1328.

[33] B. Ravelo, “Multiphysics Model of Microstrip Structure Under High Voltage Pulse Excitation,” IEEE Journal on Multiscale and Multiphysics Computational Techniques (JMMCT), Vol. 3, No. 1, Dec. 2018, pp. 88-96.

[34] Z. Xu, B. Ravelo, O. Maurice, “Multiphysics Tensorial Network Analysis Applied to PCB Interconnect Fatigue Under Thermal Cycle Aggression,” IEEE Transactions on Electromagnetic Compatibility, Vol. 61, No. 4, Aug. 2019, pp. 1253-1260.

[35] Thermal room specifications, ESPEC, available online, https://www.espec.cn